MLL3/4 methyltransferases regulate the differentiation of pluripotent stem cells via cellular respiration

Suza Mohammad Nur[1,3], Yunbo Jia[1], Muyi Ye[1], Caylin A. Lepak[1], Issam Ben-Sahra[4,5], and Kaixiang Cao[1,2,3,*]

[1]Department of Biochemistry, Case Western Reserve University

[2]Department of Genetics and Genome Sciences, Case Western Reserve University

[3]Case Comprehensive Cancer Center, Case Western Reserve University, Cleveland, OH 44106, USA

[4]Department of Biochemistry and Molecular Genetics, Northwestern University

[5]Robert H. Lurie Comprehensive Cancer Center, Northwestern University, Chicago, IL 60611, USA

Running title: MLL3/4 regulate cellular respiration to facilitate pluripotent stem cell differentiation

Keywords: MLL3, MLL4, stem cells, differentiation, cellular metabolism, glycolysis, TCA cycle

*Correspondence should be sent to the following address:

Kaixiang Cao, PhD

Department of Biochemistry, School of Medicine, Case Western Reserve University

10900 Euclid Avenue, Cleveland, OH 44106, USA

Office: (216) 368-1218

Email: kxc725@case.edu

Abstract

Enhancer-regulating epigenetic modifiers play critical roles in normal physiological processes and human pathogenesis. The major enhancer regulator paralogs MLL3 and MLL4 (MLL3/4) belong to the lysine methyltransferase 2 (KMT2) family, which catalyzes the methylation of lysine 4 on histone H3 (H3K4me). MLL3/4 are required for enhancer activation and are essential for mammalian development and stem cell differentiation. Recent studies have linked MLL3/4 with different metabolic pathways in the context of stem cell self-renewal and cancer cell growth; however, the underlying mechanisms remain elusive. Here, we utilize Seahorse extracellular flux analysis, stable isotope tracing, stem cell biology techniques, and transcriptomic analysis to investigate the functional relationship of MLL3/4, cellular respiration, and stem cell differentiation. Our results indicate that the loss of MLL3/4 impairs glycolytic activity and mitochondrial respiration in murine embryonic stem cells by downregulating the rate-limiting glycolytic enzyme Hexokinase 2 (HK2) and impairing the function of the Alpha-ketoglutarate dehydrogenase (OGDH) complex. Furthermore, simultaneously overexpression of HK2 and OGDH rescues defects in both cellular respiration and differentiation caused by MLL3/4 loss. Taken together, our study reveals a novel mechanism by which epigenetic machineries such as MLL3/4 govern the differentiation of pluripotent stem cells and facilitates the understanding of disease pathogenesis driven by enhancer malfunction.

Introduction

Enhancer deregulation is a major driver of human congenital disorders (*1-4*). In mammals, nucleosomes at enhancers are mono-methylated on lysine 4 of histone H3 (H3K4) by the paralogous enzymes Mixed-lineage Leukemia 3 (MLL3, also known as KMT2C) and Mixed-lineage Leukemia 4 (MLL4, also known as KMT2D) (*5-9*). Mice null for MLL4 die shortly after gastrulation, while MLL3 loss leads to neonatal lethality (*10, 11*). Heterozygous loss-of-function mutations in MLL4 lead to Kabuki syndrome (*1*) and those in MLL3 cause Kleefstra syndrome 2 (*4, 12, 13*). Both disorders are characterized by craniofacial dysmorphism and developmental delay, highlighting the instructive role of MLL3/4 in normal development and human pathogenesis. However, the underlying mechanisms remain poorly understood.

Recent results have revealed a functional link between MLL3/4 and cellular metabolism. MLL3/4 and nucleotide synthesis pathways co-regulate the self-renewal of pluripotent stem cells (PSCs) (*14*). Moreover, steady-state levels of glycolytic metabolites such as glucose-6-phosphate (G6P) and fructose-6-phosphate (F6P), and tricarboxylic acid (TCA) cycle metabolites including succinate, fumarate, and malate, are reduced in PSCs lacking MLL3/4 (*14*). In contrast, MLL4-deficient lung cancer and melanoma cells adopt upregulated glycolysis (*15, 16*), suggesting a context-dependent role of MLL3/4 in regulating cellular metabolism. How MLL3/4 modulate metabolic pathways and whether they govern cell fate via these pathways are largely unknown.

Cellular respiration is tightly regulated in PSCs. Naive PSCs, such as murine embryonic stem cells (ESCs), exhibit metabolic bivalency, utilizing both glycolysis and mitochondrial respiration for energy production, whereas primed PSCs are predominantly glycolytic (*17*). On the other hand, somatic cells are more dependent on mitochondrial respiration (*18, 19*). Inhibition of glycolysis drives the exit from pluripotency, while stimulation of glycolysis enhances somatic cell

66 reprogramming to induced PSCs (iPSCs) (*18, 20*), suggesting that the balance between glycolysis
67 and mitochondrial respiration instructs cell fate transition. To date, how metabolic states are
68 established during development and whether they instruct cell identity remain enigmatic.

69 To investigate the functional relationship of MLL3/4, cellular metabolism, and PSC
70 differentiation, we examined the impact of MLL3/4 loss on cellular respiration in ESCs. Both
71 extracellular acidification rate (ECAR) and oxygen consumption rate (OCR) are reduced in
72 MLL3/4-null ESCs. Stable isotope tracing reveals a reduction of metabolite levels in both
73 glycolysis and the TCA cycle upon MLL3/4 loss. MLL3/4 are required for the expression of
74 Hexokinase 2 (HK2) and for proper lipoylation of Dihydrolipoamide S-Succinyltransferase
75 (DLST), the E2 subunit of the Alpha-ketoglutarate Dehydrogenase complex (OGDHc). Moreover,
76 simultaneous overexpression of HK2 and OGDH partially rescues defects in cellular respiration
77 and differentiation caused by MLL3/4 loss. Our results provide novel insight into understanding
78 the crosstalk between epigenetic machineries and cellular metabolism. Importantly, they may pave
79 the way for developing novel strategies to target human diseases driven by enhancer deregulation.
80

Results

MLL3/4 loss dampens glycolytic activity in ground-state ESCs

We previously showed that steady-state levels of glycolysis-related metabolites, such as G6P and F6P, were reduced by the loss of MLL3/4 in ESCs (*14*), suggesting that MLL3/4 may regulate glycolysis in naive PSCs. To determine the impact of MLL3/4 loss on the rate of glycolysis, we measured the ECAR of wildtype (WT) and MLL3/4 double knockout (DKO) ESCs (*14*) with the glycolysis stress test using the Seahorse XF Analyzer. The levels of glycolysis and glycolytic capacity were significantly reduced by MLL3/4 loss (Fig. 1A-C), suggesting that MLL3/4 are required to maintain glycolytic activity in naive PSCs. To understand if the decrease in the steady-state levels of metabolites reflects altered glycolytic activity, we performed stable isotope tracing with [$^{13}C_6$]-glucose in WT and MLL3/4 DKO ESCs, followed by liquid chromatography-tandem mass spectrometry (LC-MS/MS) analysis (Fig. 1D). Consistent with results in steady-state metabolomics, the incorporation of ^{13}C into F6P/G1P (glucose-1-phosphate)/G6P (m+6) was significantly reduced by MLL3/4 loss (Fig. 1E and Fig. S1A). Moreover, levels of lactate (m+3) were reduced by MLL3/4 loss (Fig. 1F and Fig. S1B), corresponding to the decreased glycolytic activity in MLL3/4 DKO ESCs. To determine if the decreased levels of glycolytic metabolites resulted from defective glucose import, we measured the rate of glucose uptake and found that MLL3/4 loss did not have a significant impact on cellular import of glucose in ESCs (Fig. 1G), suggesting that MLL3/4 loss impairs early rate-limiting steps in glycolysis, leading to reduced glycolytic activity in ESCs.

To elucidate the mechanism underlying reduced rates of glycolysis in MLL3/4 DKO ESCs, we analyzed RNA-seq data (*14*) to examine the expression levels of genes encoding glycolytic enzymes involved in G6P and F6P metabolism. We found that *Hk2*, the gene encoding the rate-

104 limiting enzyme Hexokinase 2 that catalyzes the phosphorylation of glucose to G6P, was
105 significantly downregulated by MLL3/4 loss (Fig. S1C). On the other hand, the expression levels
106 of genes encoding Glucose-6-phosphate isomerase (*Gpi1*), Phosphofructokinase 1 (*Pfkl* and *Pfkp*),
107 and Phosphofructokinase 2 (*Pfkfb1* and *Pfkfb2*) were comparable between WT and MLL3/4 DKO
108 ESCs (Fig. S1C). We then measured the levels of Hexokinases in WT and MLL3/4 DKO ESCs by
109 western blotting. HK2 levels were reduced by the loss of MLL3/4, while the levels of HK1
110 (Hexokinase 1), the paralog of HK2, remained largely unchanged (Fig. 1H). To investigate how
111 MLL3/4 regulate the expression levels of *Hk2*, we analyzed ChIP-seq datasets (*7, 14*) and found
112 at least six putative enhancers near the *Hk2* locus that are bound by MLL4 and exhibit reduced
113 H3K27ac levels upon MLL3/4 loss (Fig. S1D), suggesting that MLL3/4 regulate *Hk2* through
114 these putative enhancers. Taken together, these data indicate that the glycolytic activity of naive
115 PSCs requires MLL3/4 and that the decreased HK2 levels may be responsible for the defective
116 glycolysis caused by MLL3/4 loss.
117
118 **MLL3/4 are required for mitochondrial respiration in ground-state ESCs**
119 The metabolic bivalency is one of the hallmarks of naive PSCs (*21, 22*). To examine the role of
120 MLL3/4 in regulating mitochondrial respiration in naive PSCs, we measured the OCR of WT and
121 MLL3/4 DKO ESCs with the mitochondrial stress assay using the Seahorse XF Analyzer.
122 Interestingly, the levels of basal and maximal respiration were significantly reduced by MLL3/4
123 loss in ESCs (Fig. 2A-C), suggesting that MLL3/4 are required to maintain the metabolic bivalency
124 in naive PSCs. Analysis of ^{13}C incorporation into TCA-cycle metabolites via stable isotope tracing
125 using [$^{13}C_6$]-glucose labeling (Fig. 2D) showed that MLL3/4 loss did not have a significant impact
126 on the levels of citrate/isocitrate (m+2) and alpha-ketoglutarate (α-KG) (m+2) (Fig. 2E-F and Fig.

127 S2A-B). In contrast, the levels of succinate (m+2), fumarate (m+2), and malate (m+2) were
128 significantly reduced in MLL3/4 DKO ESCs (Fig. 2G-I and Fig. S2C-E), suggesting that potential
129 disruptions in TCA cycle steps downstream of α-KG contribute to the impaired mitochondrial
130 respiration driven by MLL3/4 loss.

131 To further examine this possibility, we performed stable isotope tracing with [$^{13}C_5$]-
132 glutamine labeling (Fig. 2J). Although MLL3/4 loss did not have a significant impact on the levels
133 of glutamate (m+5) (Fig. 2K and Fig. S2F), the levels of α-KG (m+5) were significantly reduced
134 in MLL3/4 DKO ESCs (Fig. 2L and Fig. S2G). This reduction may reflect impaired conversion of
135 glutamate to α-KG, although the expression levels of *Glud1*, which encodes Glutamate
136 Dehydrogenase (GDH), the enzyme catalyzing the conversion of glutamate to α-KG, were
137 comparable between WT and MLL3/4 DKO ESCs (Fig. S2L). Consistent with results from [$^{13}C_6$]-
138 glucose labeling, the levels of succinate (m+4), fumarate (m+4), and malate (m+4) were
139 significantly reduced in MLL3/4 DKO ESCs, while those of citrate/isocitrate (m+4) were largely
140 unchanged after [$^{13}C_5$]-glutamine labeling (Fig. 2M-P and Fig. S2H-K). Furthermore, expression
141 levels of multiple genes encoding enzymes involved in α-KG and downstream TCA cycle
142 metabolism were comparable between MLL3/4 DKO and WT ESCs (Fig. S2L). In addition,
143 protein levels of OGDH, SUCLA2, SUCLG1, SUCLG2, and SDHA remained largely unperturbed
144 upon MLL3/4 loss (Fig. S2M-O), suggesting that MLL3/4 regulate TCA cycle metabolites via
145 mechanisms other than transcriptional control of metabolic enzymes. Taken together, these results
146 demonstrate that MLL3/4 loss impairs mitochondrial respiration and disrupts metabolic flux at
147 specific steps within the TCA cycle in naive PSCs.
148

149 **Simultaneous overexpression of HK2 and OGDH rescues defects in cellular respiration**
150 **caused by MLL3/4 loss**

151 To determine if MLL3/4 regulate cellular respiration in ESCs through activating HK2, we
152 overexpressed 3×HA-tagged HK2 in MLL3/4 DKO ESCs with a doxycycline (DOX)-inducible
153 system (*23, 24*) (Fig. S3A). HK2 overexpression increased glycolytic activity in MLL3/4 DKO
154 cells (Fig. S3B-D); however, OCR during basal respiration was reduced upon HK2 expression (Fig.
155 S3E-G), suggesting that HK2 overexpression renders MLL3/4 DKO ESCs more dependent on
156 glycolysis for energy production.

157 Since HK2 overexpression led to an expected increase in ECAR but a reduction in OCR,
158 we sought to restore both glycolysis and mitochondrial respiration in MLL3/4 DKO ESCs to study
159 the functional relationship of MLL3/4, cellular respiration, and the differentiation capability of
160 PSCs. We hypothesized that the decrease of ^{13}C incorporation in succinate, fumarate, and malate
161 in both [$^{13}C_6$]-glucose and [$^{13}C_5$]-glutamine labelled MLL3/4-null ESCs results from the
162 potentially defective OGDHc caused by the loss of MLL3/4. Although OGDH levels were
163 comparable between MLL3/4 DKO and WT ESCs, OGDH overexpression could potentially
164 compensate for reduced levels of succinate, fumarate, and malate in MLL3/4-null ESCs. We
165 therefore simultaneously overexpressed 3×HA-tagged HK2 and 3×FLAG-tagged OGDH in
166 MLL3/4 DKO ESCs using DOX-inducible expression vectors carrying distinct drug resistance
167 genes (Fig. 3A). Increased levels of HK2 and OGDH led to elevated rates of glycolysis, glycolytic
168 capacity, and both basal and maximal respiration (Fig. 3B-G). Furthermore, stable isotope tracing
169 by labeling MLL3/4 DKO and HK2/OGDH double-overexpressing (DOE) MLL3/4 DKO cells
170 with [$^{13}C_6$]-glucose indicated that the levels of metabolites reduced by MLL3/4 loss such as
171 F6P/G1P/G6P (m+6), lactate (m+3), succinate (m+2), and fumarate (m+2) were partially restored

172 by HK2/OGDH DOE (Fig. 3H-M, Fig. S4A-B, and Fig. S4E-G). As expected, we did not observe
173 a significant difference in the levels of citrate/isocitrate (m+2) or α-KG (m+2) (Fig. 3J and Fig.
174 S4C-E). Notably, malate (m+2) levels were not significantly increased upon HK2/OGDH DOE in
175 MLL3/4 DKO cells (Fig. 3M and Fig. S4H), suggesting that there are additional regulatory layers
176 on the levels of malate besides HK2 and OGDHc.

177 Our results that HK2/OGDH overexpression rescues defects in cellular respiration and
178 levels of glycolytic and TCA cycle metabolites suggest that MLL3/4 may regulate glycolysis and
179 mitochondrial respiration through activating *Hk2* expression and maintaining the normal function
180 of the OGDHc. To further elucidate the molecular mechanisms by which MLL3/4 regulate the
181 TCA cycle, we examined the levels of DLST and Dihydrolipoamide Dehydrogenase (DLD), E2
182 and E3 components of the OGDHc. MLL3/4 loss had little impact on their levels (Fig. 3N-O),
183 suggesting that MLL3/4 are unlikely to regulate mitochondrial respiration via modulating the
184 abundance of OGDHc components. Lipoylated DLST is essential for the conversion of α-KG to
185 succinyl-CoA (*25-27*). To understand if MLL3/4 loss impairs the activity of DLST, we examined
186 the levels of lipoylated proteins in WT and MLL3/4 DKO ESCs using a specific anti-lipoate
187 antibody (*28*). MLL3/4 loss led to a reproducible decrease of the lipoylated protein species with
188 lower molecular weight, attributed to lipoylated DLST based on its size (Fig. 3P). The decrease in
189 lipoylation was specific to DLST as levels of other abundantly lipoylated proteins in the
190 mitochondria, such as Dihydrolipoamide Acetyltransferase (DLAT) in the Pyruvate
191 Dehydrogenase complex and Dihydrolipoamide Branched-chain Transacylase (DBT) in the
192 Branched-chain Alpha-keto Acid Dehydrogenase complex (*26, 27*), were comparable in MLL3/4
193 DKO and WT ESCs (Fig. 3P). Taken together, these results suggest that MLL3/4 regulate cellular
194 respiration by maintaining the levels of HK2 and the activity of OGDHc in naive PSCs, and that

195 simultaneous overexpression of HK2 and OGDH partially rescues defects in cellular respiration
196 caused by MLL3/4 loss.
197
198 **Simultaneous overexpression of HK2 and OGDH rescues differentiation defects caused by**
199 **MLL3/4 loss**
200 To assess the impact of MLL3/4 loss on cell fate transition, we generated embryoid bodies (EBs)
201 from WT and MLL3/4 DKO ESCs. As expected, MLL3/4 loss led to a decrease in the size of day
202 6 EBs (Fig. 4A-B), indicating that MLL3/4 are required for PSC differentiation. RNA-seq analysis
203 showed that MLL3/4 loss caused the significant deregulation of 4,547 genes in day 6 EBs (Fig.
204 4C). Among genes significantly downregulated in MLL3/4 DKO EBs, 52.3% (1,192 of 2,280)
205 were significantly upregulated during WT EB differentiation (Fig. 4D), suggesting that these genes
206 are dependent on MLL3/4 to be activated during differentiation. We thus defined them as MLL3/4-
207 dependent differentiation genes. Gene ontology (GO) analysis showed that the top 300 upregulated
208 genes of the 1,192 MLL3/4-dependent differentiation genes were enriched for embryogenesis-
209 related genes and known MLL4 targets essential for actin cytoskeleton organization (*7*) (Fig. 4E),
210 further indicating that MLL3/4 loss impairs PSC differentiation. Indeed, pluripotency genes were
211 significantly upregulated in MLL3/4 DKO EBs and marker genes of meso- and endo-derm
212 lineages were downregulated in EBs by MLL3/4 loss (Fig. S5A-B). These data demonstrate that
213 MLL3/4 are required for PSC differentiation and related transcriptional reconfiguration.
214 To examine if the partial restoration of cellular respiration had any impact on the
215 differentiation capacity of ESCs lacking MLL3/4, we treated MLL3/4 DKO and HK2/OGDH DOE
216 MLL3/4 DKO cells with DOX and differentiated them toward EBs. EB differentiation revealed
217 that HK2/OGDH DOE led to a significant increase in the size of day 6 EBs (Fig. 4F-G), suggesting

218 that restoring cellular respiration rescues differentiation defects caused by MLL3/4 loss. Moreover,
219 RNA-seq analysis identified 1,778 significantly deregulated genes by HK2/OGDH DOE
220 compared with MLL3/4 DKO ESCs treated with DOX (Fig. 4H). Gene set enrichment analysis
221 (GSEA) and hierarchical clustering analysis of MLL3/4-dependent differentiation genes (Fig. 4D)
222 revealed a significant upregulation of them upon HK2/OGDH DOE (Fig. 4I-J). Indeed, 34.3% of
223 genes upregulated by HK2/OGDH DOE (300 of 875) were dependent on MLL3/4 to be activated
224 during differentiation (Fig. 4K), suggesting that the impaired cellular respiration contributes to
225 differentiation defects caused by MLL3/4 loss. GO analysis of the 300 significantly rescued genes
226 showed enrichment of genes related to embryo morphogenesis and mesodermal development such
227 as the development of renal and skeletal systems (Fig. 4L). Consistently, HK2/OGDH DOE led
228 to the significant downregulation of pluripotency genes and the significant upregulation of
229 differentiation marker genes (Fig. S5C-D). Taken together, these results suggest that defects in
230 cellular respiration contribute to differentiation failures of naive PSCs lacking MLL3/4.
231

232 **Discussion**

233 Epigenetic regulators, including histone modifiers, play central roles in regulating cell fate
234 transition during PSC differentiation, somatic cell reprogramming, and normal development (*29-*
235 *35*); however, the underlying mechanisms remain incompletely understood, in part because many
236 epigenetic regulators function independently of their catalytic activity (*6, 7, 24, 36-43*). Besides
237 being essential for cellular differentiation and mammalian embryogenesis (*11, 44*), loss-of-
238 function mutations in MLL3 and MLL4 drive congenital disorders such as Kleefstra syndrome 2
239 and Kabuki syndrome, as well as multiple types of cancer (*1, 4, 13, 45*). Recent advances reveal a
240 novel link between MLL3/4 and cellular metabolism; however, whether and how the roles of
241 MLL3/4 in regulating cell fate and metabolic pathways intersect are unclear. Here, we unveil a
242 previously unrecognized function of MLL3/4 in regulating glycolysis and mitochondrial
243 respiration in murine ESCs. Our findings suggest that MLL3/4 govern cell fate transition during
244 the differentiation of naive PSCs through regulating the expression levels of *Hk2* and the function
245 of OGDHc, two rate-limiting nodes in glycolysis and the TCA cycle, respectively. Importantly,
246 restoring defective cellular respiration may be an effective strategy to treat diseases driven by
247 MLL3/MLL4 loss-of-function.

248 We find that MLL3/4 loss causes decreased glycolytic activity and mitochondrial
249 respiration in ESCs. Metabolic bivalency is a defining feature of naive PSCs such as murine ESCs
250 (*22*). The decrease of glycolytic activity in MLL3/4 null cells may hinder the cells from exiting
251 naive pluripotency, as formative PSCs and primed PSCs are highly glycolytic (*17*). On the other
252 hand, inhibiting glycolysis promotes differentiation as somatic cells have much elevated levels of
253 oxidative phosphorylation compared with PSCs (*18-20*). Therefore, the dampened mitochondrial
254 respiration caused by MLL3/4 loss may impair the differentiation of PSCs into germ layers and/or

255 specific lineages. Our data provide a mechanistic explanation for the failure of MLL4-null ESCs
256 to exit naive pluripotency and for the severe gastrulation defects observed in MLL3/4-null embryos
257 (*7, 10, 46*).

258 Our data support that MLL3/4 facilitate glycolysis in naive ESCs through maintaining the
259 expression of *Hk2*, which encodes the rate-limiting enzyme Hexokinase 2 in glycolysis. It is likely
260 that MLL3/4 regulate *Hk2* expression through enhancers as we identified multiple putative *cis*-
261 regulatory regions that may be directly regulated by MLL3/4. Understanding whether and how
262 MLL3/4 function through these enhancers to control the expression levels of *Hk2* is an interesting
263 topic. Shadow enhancers have been reported in different organisms including *Drosophila*, mouse,
264 and human (*47-49*). Generating individual and compound enhancer mutations will elucidate how
265 the putative enhancers regulate *Hk2*. Combination of MLL3/4 loss-of-function mutations and
266 enhancer mutants will further reveal the functional relationship between MLL3/4 and putative
267 enhancers in regulating *Hk2*. These future studies are essential for understanding the mechanisms
268 by which MLL3/4 regulate glycolysis in naive PSCs.

269 Interestingly, overexpressing HK2 alone only partially restores glycolytic activity in ESCs
270 lacking MLL3/4, suggesting that MLL3/4 support glycolysis in naive PSCs through additional
271 mechanisms. Determining whether other critical regulators of glycolysis such as
272 Phosphofructokinase, Pyruvate Kinase, and Lactate Dehydrogenase play a role in dampening
273 glycolysis in the context of MLL3/4 loss-of-function is an important future study. Genome-wide
274 and targeted genetic screens may also identify additional factors that rescue glycolysis in MLL3/4-
275 null ESCs. It is noteworthy that HK2 overexpression leads to a decrease of OCR in MLL3/4 DKO
276 ESCs, suggesting that these cells are more dependent on glycolysis as an energy source in
277 comparison to oxidative phosphorylation under high levels of HK2. Since steady-state acetyl-CoA

278 levels were reduced in MLL3/4 DKO ESCs (*14*) and our stable isotope tracing assays were not
279 able to detect acetyl-CoA, it is interesting to examine if and how MLL3/4 loss affects the
280 mitochondrial transport of pyruvate in ESCs in the future. Defining the role of MLL3/4 in other
281 pathways leading to the synthesis of acetyl-CoA such as fatty acid metabolism may also facilitate
282 understanding how MLL3/4 regulate the conjunction of glycolysis and the TCA cycle.

283 The reduction in the ^{13}C incorporation into succinate, fumarate, and malate in both [$^{13}C_6$]-
284 glucose and [$^{13}C_5$]-glutamine labeling of MLL3/4 DKO ESCs suggests a functionally defective
285 OGDHc caused by MLL3/4 loss. Indeed, the levels of lipoylated DLST were decreased in
286 MLL3/4-null cells, suggesting a reduced activity of the OGDHc. It is likely that the decrease of
287 lipoylation is specific to DLST as MLL3/4 loss has little impact on the levels of lipoylated DLAT.
288 It was previously shown that the α/β hydrolase ABHD11 binds OGDHc and maintains the activity
289 of lipoylated DLST by preventing the formation of lipoyl adducts (*28*). It will be interesting to
290 investigate the functional relationship between MLL3/4, ABHD11, and OGDHc in the future to
291 understand how MLL3/4 regulate the activity of OGDHc. It is also noteworthy that the levels of
292 ^{13}C incorporation into α-KG (m+5) is impaired in MLL3/4 DKO ESCs in the [$^{13}C_5$]-glutamine
293 labeling experiments, although α-KG (m+2) levels through [$^{13}C_5$]-glucose labeling and steady-
294 state levels of α-KG were largely unchanged by MLL3/4 loss (*14*). Besides Glutamate
295 Dehydrogenase, Glutamate Pyruvate Transaminase and Glutamate Oxaloacetate Transaminase
296 also can convert glutamate to α-KG. Future studies on the role of MLL3/4 in regulating the
297 conversion of glutamate to α-KG would be important to understand the crosstalk between MLL3/4
298 and glutaminolysis.

299 α-KG is an essential co-substrate of Fe(II)/α-KG-dependent dioxygenases including
300 Jumonji C (JmjC) domain-containing histone demethylases and the ten-eleven translocation (TET)

301 family of DNA hydroxylases (*50, 51*), playing a role in regulating the levels of methylation on
302 different lysine residues of histones and 5-methyl Cytosine (5mC) on DNA in mammalian cells.
303 Due to their structural similarity to α-KG, 2-hydroxyglutarate, succinate, and fumarate inhibit α-
304 KG-dependent dioxygenases by acting as a competitive inhibitor of α-KG (*52, 53*). Our results
305 that MLL3/4 loss in ESCs lead to a decreased levels of succinate and fumarate, through steady-
306 state metabolomics and stable isotope tracing with [$^{13}C_6$]-glucose and [$^{13}C_5$]-glutamine, suggest a
307 possibility that the activities of multiple histone demethylases and TETs are increased in cells with
308 MLL3/4 loss-of-function. Such a possibility provides a mechanistic explanation for the DNA
309 hypomethylation observed in MLL4-depleted B cells in mouse and MLL4 mutant prostate cancers
310 in human (*54*). Understanding the impact of the potential alterations in the levels of histone
311 methylation and DNA methylation on the differentiation capability of MLL3/4-mutant PSCs is
312 very interesting and may provide insight into understanding the molecular mechanisms underlying
313 the functional relationship of cellular respiration, epigenetic machineries, and cell fate transition.
314 In summary, our study reveals a previously unappreciated crosstalk between epigenetic
315 modifiers exemplified by MLL3/4 and cellular respiration pathways glycolysis and the TCA cycle
316 in regulating cell fate. Our findings on MLL3/4 regulating the levels of HK2 and lipoylated DLST
317 could pave the way for designing therapeutic strategies to target human diseases driven by loss-
318 of-function mutations of MLL3/4.
319

320 **Methods**

321 **Antibodies**

322 The following primary antibodies were used in this study: anti-HK2 (Cell Signaling Technology
323 2867), anti-HK1 (Cell Signaling Technology 2024), anti-OGDH (Proteintech 17110-1-AP), anti-
324 SDHA (Abcam 14715), anti-SUCLA2 (Proteintech 12627-1-AP), anti-SUCLG1 (Proteintech
325 14923-1-AP), anti-SUCLG2 (Proteintech NBP1-32521), anti-FLAG (MiliporeSigma F3165),
326 anti-HA (MiliporeSigma H3663), anti-DLST (Cell Signaling Technology 5556), anti-DLD (Santa
327 Cruz 365977), anti-Lipoic acid (Calbiochem 437695), anti-Tubulin (Developmental Studies
328 Hybridoma Bank E7), and anti-HSP90 (Santa Cruz 13119).

329

330 **ESC Culture and EB differentiation**

331 ESCs were cultured in serum-free medium supplemented with 2i/LIF as previously described (*55*).
332 For the generation of HK2 overexpressing and HK2/OGDH DOE MLL3/4 DKO ESCs, cells were
333 transfected with DOX-inducible PiggyBac vectors (*23*) as previously described (*24*) using an
334 Amaxa Nucleofector (Lonza). EB differentiation was performed using the hanging-drop method
335 as previously described (*24*). For DOX-induced overexpression, ESCs were treated with 100 ng/ml
336 doxycycline for 48 hours prior to downstream assays. For differentiation experiments, doxycycline
337 (100 ng/ml) were added 24 hours prior to EB formation and maintained throughout the 6-day
338 differentiation period.

339

340 **Seahorse extracellular flux assays**

341 ESCs were seeded in Seahorse XF microplates (Agilent) and cultured overnight with 2i/LIF serum-
342 free medium. Cells were then incubated in Seahorse XF assay medium (Agilent) at 37°C in a non-

343 CO_2 incubator for 1 hour. For the Glycolysis Stress Test (Agilent 103020-100), glucose (10mM),
344 oligomycin (2 μM), and 2-DG (50mM) were sequentially injected. For the Mitochondrial Stress
345 Test (Agilent 103015-100), oligomycin (1.5 μM), FCCP (0.5 μM), and Rot/AA (0.5 μM) were
346 sequentially injected. Cell Titer Glo assay (Promega) was performed in parallel on replica plates
347 to determine the cell number of each well. Individual raw ECAR and OCR values recorded by the
348 Seahorse XF Analyzer were normalized against the average Cell Titer Glo values of control wells
349 to derive normalized ECAR and normalized OCR values. Wave software (Agilent) was used to
350 extract individual ECAR and OCR measurements, which were subsequently used to generate the
351 bar plots.
352
353 **Stable isotope tracing and metabolomics**
354 Stable isotope labeling and metabolite extraction were performed as previously described (*14*).
355 ESCs were incubated with media containing 25 mM [$^{13}C_6$]-glucose or 4mM [$^{13}C_5$]-glutamine for
356 2 hours before methanol extraction. Metabolomic analyses were performed at the Northwestern
357 Metabolomics Core Facility.
358
359 **Glucose uptake assay**
360 Glucose update was measured using the Glucose Uptake-Glo Assay Kit (Promega J1342)
361 according to the manufacturer's instructions. In brief, 2×10^4 cells were seeded on each well of a
362 96-well flat bottom plate with opaque walls and clear bottoms (Corning 7200587). After 16 hours
363 of culture, cells were incubated in glucose-free medium for 1 hour at 37°C in the tissue-culture
364 incubator. Cells were then treated with 1mM 2-DG for 10 minutes at room temperature, followed
365 by the treatment of stop buffer, neutralization buffer, and detection reagent following the

366 instructions of the manufacturer. After 2.5 hours of dark-conditioned incubation, the luminescence
367 was measured using a GloMax luminometer (Promega). The luminescence data were normalized
368 by cell numbers measured with the Cell Titer Glo assay (Promega) on replica plates in parallel.
369

370 **RNA-seq and analysis**

371 Total RNA was extracted using TRIzol reagent (Thermo Fisher) following the manufacturer's
372 instructions. Each cell line was analyzed in at least two biological replicates. Extracted RNA were
373 treated with DNase I (Sigma) and purified with the RNeasy Plus Mini Kit (Qiagen). Ribosomal
374 RNA was removed from the purified RNA with the NEBNext rRNA Depletion Kit (New England
375 BioLabs). RNA libraries were then prepared with the NEBNext Ultra II Directional RNA Library
376 Prep Kit (New England BioLabs). The pooled libraries were sequenced with 150 bp paired-end
377 reads on the NovaSeq platfrom (Illumina).

378 Raw reads were processed with Trimmomatic v0.39(*56*) to remove adaptors and low-
379 quality reads with the parameter "-q 30". The cleaned reads were aligned to the mm9 genome
380 assembly using STAR v2.5.1 with default parameter (*57*). Reads were normalized to total read
381 counts per million (cpm) and visualized as bigwig-formatted coverage tracks using deepTools
382 v3.5.6 (*58*). Gene expression was quantified using HTseq V2.0.2 (*59*), and differential gene
383 expression analysis was performed with EdgeR v4.0.16 (*60*). Significantly differentially expressed
384 genes were identified with Benjamini-Hochberg-adjusted p value cutoff < 0.01 and a log fold
385 change threshold greater than |1|. hierarchical clustering heatmaps were generated using the ggpubr
386 v0.6.0 (https://rpkgs.datanovia.com/ggpubr/). GSEA plots were generated with clusterProfiler
387 v4.10.1 (*61*). Gene ontology (GO) analysis was performed using Metascape v3.5.20260201 (*62*).
388

Acknowledgements

We thank the Cao lab members for their helpful suggestions and discussions. We thank Dr. Peng Gao and the Northwestern Metabolomics Core Facility for performing the metabolomics study. We thank Emmalee W. Cooke for technical support. We thank Yalu Zhou for bioinformatic analysis support. This study was supported in part by grants R35GM150668, R00HD094906, and P30CA043703 from the National Institutes of Health to K.C.

Author contributions

K.C. conceived the study. S.M.N., I.B., and K.C. designed the research. S.M.N., Y.J., and M.Y. performed experiments. S.M.N., Y.J., M.Y., and K.C. analyzed the data. S.M.N. and K.C. wrote the manuscript. C.L. and I.B. critically read the manuscript.

401 **Figure legends**

402 **Figure 1. The loss of MLL3/4 leads to impaired glycolytic activity in ground-state ESCs.**

403 (A) Representative ECAR traces of WT and MLL3/4 DKO ESCs measured by the Seahorse XF
404 glycolysis stress test assay. Data were normalized by the number of cells at the time of the assay
405 and are represented as mean ± S.D. Each data point had six replicates, and the experiment was
406 repeated three times independently. 2-DG: 2-Deoxy-D-glucose.

407 (B-C) Bar plots of ECAR showing the levels of glycolysis (B) and glycolytic capacity (C) in WT
408 and MLL3/4 DKO ESCs. Data are presented as mean ± S.D. p-values were calculated using
409 Student's t-test.

410 (D) Schematic of glycolysis illustrating the fate of ^{13}C carbons upon the incubation with [$^{13}C_6$]-
411 glucose.

412 (E-F) Bar plots showing the levels of F6P/G1P/G6P (m+6, E) and lactate (m+3, F) in WT and
413 MLL3/4 DKO ESCs labeled with [$^{13}C_6$]-glucose. n=3 biological replicates per sample. Data are
414 presented as mean ± S.D. p-values were calculated using Student's t-test.

415 (G) Bar plots showing the levels of glucose uptake in WT and MLL3/4 DKO ESCs. n=6 replicates
416 per sample. Experiments were repeated three times independently and representative results were
417 shown. Data were normalized by the number of cells at the time of the assay and are presented as
418 mean ± S.D. p-values were calculated using Student's t-test. RLU: relative light unit.

419 (H) Western blots showing the levels of HK1 and HK2 in WT and MLL3/4 DKO ESCs. 10 and
420 20μg of cell lysates were loaded for each sample. Experiments were repeated three times
421 independently and representative results were shown. Protein levels in each lane were quantified
422 by normalizing with Tubulin signals of the corresponding lane.

423

424 **Figure 2. The loss of MLL3/4 leads to impaired mitochondrial respiration in ground-state**
425 **ESCs.**
426 (A) Representative OCR traces of WT and MLL3/4 DKO ESCs measured by the Seahorse XF
427 mitochondrial stress test assay. Data were normalized by the number of cells at the time of the
428 assay and are represented as mean ± S.D. Each data point had six replicates, and the experiment
429 was repeated three times independently. FCCP: Carbonyl Cyanide-4-(trifluoromethoxy)
430 phenylhydrazone. ROT/AA: Rotenone and Antimycin A.
431 (B-C) Bar plots showing the levels of OCR during basal (B) and maximal (C) respiration in WT
432 and MLL3/4 DKO ESCs. Data are presented as mean ± S.D. p-values were calculated using
433 Student's t-test.
434 (D) Schematic of the TCA cycle illustrating the fate of ^{13}C carbons upon the incubation with [$^{13}C_6$]-
435 glucose.
436 (E-I) Bar plots showing levels of citrate/isocitrate (m+2, E), α-KG (m+2, F), succinate (m+2, G),
437 fumarate (m+2, H), and malate (m+2, I) in WT and MLL3/4 DKO ESCs labeled with [$^{13}C_6$]-
438 glucose. n=3 biological replicates per sample. Data are presented as mean ± S.D. p-values were
439 calculated using Student's t-test.
440 (J) Schematic of the TCA cycle illustrating the fate of ^{13}C carbons upon the incubation with [$^{13}C_5$]-
441 glutamine.
442 (K-P) Bar plots showing levels of glutamate (m+5, K), α-KG (m+5, L), succinate (m+4, M),
443 fumarate (m+4, N), malate (m+4, O), and citrate/isocitrate (m+4, P) in WT and MLL3/4 DKO
444 ESCs labeled with [$^{13}C_5$]-glutamine. n=3 biological replicates per sample. Data are presented as
445 mean ± S.D. p-values were calculated using Student's t-test.
446

447 **Figure 3. Simultaneous overexpression of HK2 and OGDH rescues metabolic defects of**
448 **MLL3/4 DKO ESCs.**

449 (A) Western blots showing levels of HK2, 3×HA-tagged HK2, OGDH, and 3×FLAG-tagged
450 OGDH in MLL3/4 DKO ESCs and MLL3/4 DKO ESCs overexpressing HK2/OGDH treated with
451 or without DOX. 10 and 20μg of cell lysates were loaded for each sample. Experiments were
452 repeated three times independently and representative results were shown. Protein levels in each
453 lane of the anti-HK2 and anti-OGDH blots were quantified by normalizing with Tubulin signals
454 of the corresponding lane.

455 (B) Representative ECAR traces of MLL3/4 DKO ESCs treated with DOX (DKO+DOX) and
456 MLL3/4 DKO ESCs overexpressing HK2/OGDH (DOE+DOX) measured by the Seahorse XF
457 glycolysis stress test assay. Data were normalized by the number of cells at the time of the assay
458 and are represented as mean ± S.D. Each data point had six replicates, and the experiment was
459 repeated three times independently.

460 (C-D) Bar plots of ECAR showing the level of glycolysis (C) and glycolytic capacity (D) in
461 MLL3/4 DKO ESCs treated with DOX (DKO+DOX) and MLL3/4 DKO ESCs overexpressing
462 HK2/OGDH (DOE+DOX). Data are presented as mean ± S.D. p-values were calculated using
463 Student's t-test.

464 (E) Representative OCR traces of MLL3/4 DKO ESCs treated with DOX (DKO+DOX) and
465 MLL3/4 DKO ESCs overexpressing HK2/OGDH (DOE+DOX) measured by the Seahorse XF
466 mitochondrial stress test assay. Data were normalized by the number of cells at the time of the
467 assay and are represented as mean ± S.D. Each data point had six replicates, and the experiment
468 was repeated three times independently.

469 (F-G) Bar plots showing the levels of OCR during basal (F) and maximal (G) respiration in
470 MLL3/4 DKO ESCs treated with DOX (DKO+DOX) and MLL3/4 DKO ESCs overexpressing
471 HK2/OGDH (DOE+DOX). Data are presented as mean ± S.D. p-values were calculated using
472 Student's t-test.
473 (H-M) Bar plots showing levels of F6P/G1P/G6P (m+6, H), lactate (m+3, I), α-KG (m+2, J),
474 succinate (m+2, K), fumarate (m+2, L), and malate (m+2, M) in MLL3/4 DKO ESCs treated with
475 DOX (DKO+DOX) and MLL3/4 DKO ESCs overexpressing HK2/OGDH (DOE+DOX) labeled
476 with [$^{13}C_6$]-glucose. n=3 biological replicates per sample. Data are presented as mean ± S.D. p-
477 values were calculated using Student's t-test.
478 (N-P) Western blots showing the levels of DLST (N), DLD (O), and lipoylated proteins (P) in WT
479 and MLL3/4 DKO ESCs. 10 and 20μg of cell lysates were loaded for each sample. Experiments
480 were repeated three times independently and representative results were shown. Protein levels of
481 DLST (in N), DLD (in O), and lipoylated DLST (in P) were quantified by normalizing with HSP90
482 signals of the corresponding lane.
483
484 **Figure 4. Simultaneous overexpression of HK2 and OGDH rescues differentiation defects**
485 **caused by MLL3/4 loss.**
486 (A) Representative images of day 6 WT and MLL3/4 DKO EBs. Scale bar: 250μm.
487 (B) Quantification of EB sizes in (A). n=50 for each genotype. Experiments were repeated three
488 times independently and representative results were shown.
489 (C) Correlation plots of RNA-seq data between day 6 MLL3/4 DKO and WT EBs. Data were
490 derived from two biological replicates. Statistical significance was determined by two-sided Wald
491 test and p-values were corrected for multiple testing using the Benjamini–Hochberg method.

492 Significantly up- and downregulated genes (adjusted $p<0.01$, $|\log FC|>1$) were labeled in red and
493 blue with numbers of genes noted, respectively.
494 (D) Venn diagram identifying 1,192 MLL3/4-dependent differentiation genes.
495 (E) GO analysis of top 300 MLL3/4-dependent differentiation genes.
496 (F) Representative images of day 6 MLL3/4 DKO EBs treated with DOX (DKO+DOX) and
497 MLL3/4 DKO EBs overexpressing HK2/OGDH (DOE+DOX). Scale bar: 250μm.
498 (G) Quantitation of EB sizes in (F). n=50 for each genotype. Experiments were repeated three
499 times independently and representative results were shown.
500 (H) Correlation plots of RNA-seq data between MLL3/4 DKO EBs treated with DOX
501 (DKO+DOX) and MLL3/4 DKO EBs overexpressing HK2/OGDH (DOE+DOX).
502 (I) GSEA analysis of MLL3/4-dependent differentiation genes (1,192 in D) comparing MLL3/4
503 DKO EBs treated with DOX (DKO+DOX) and MLL3/4 DKO EBs overexpressing HK2/OGDH
504 (DOE+DOX). RES: running enrichment score; RLM: ranked list metric; NES: normalized
505 enrichment score; FDR: false discovery rate.
506 (J) Hierarchical clustering analysis of the expression levels of 1,192 MLL3/4-dependent
507 differentiation genes in MLL3/4 DKO EBs treated with DOX (DKO+DOX) and MLL3/4 DKO
508 EBs overexpressing HK2/OGDH (DOE+DOX). FPKM: Fragments per kilobase of transcript per
509 million mapped reads.
510 (K) Venn diagram showing the overlap of MLL3/4-dependent differentiation genes and
511 significantly upregulated genes in MLL3/4 DKO EBs overexpressing HK2/OGDH (red in H).
512 (L) GO analysis of 300 DOE-rescued differentiation genes (overlapping genes in K).
513

514 **Figure S1. The impact of MLL3/4 loss on glycolytic metabolites, glycolytic gene expression,**
515 **and putative enhancers at the *Hk2* locus.**
516 (A-B) Stable isotope tracing of WT and MLL3/4 DKO ESCs labeled with [$^{13}C_6$]-glucose. The
517 levels of isotopologues (m+0 to m+6) of F6P/G6P/G1P (A) and lactate (B) were shown as stacked
518 bar plots.
519 (C) Relative expression levels of genes coding key glycolytic enzymes involved in the anabolism
520 and catabolism of G6P, F6P, and lactate. CPM (counts per million reads) from RNA-seq data (*14*)
521 of MLL3/4 DKO ESCs were normalized to those of WT ESCs. p-values were determined by two-
522 sided Wald test and corrected using the Benjamini–Hochberg method.
523 (D) Genome browser view of MLL4 ChIP-seq signals in WT ESCs, and that of H3K27ac and
524 H3K4me3 ChIP-seq signals in WT and MLL3/4 DKO ESCs at the *Hk2* locus. Putative enhancers
525 bound by MLL4 around *Hk2* gene were highlighted.
526
527 **Figure S2. The impact of MLL3/4 loss on TCA-cycle metabolites and the expression of TCA-**
528 **cycle-related genes.**
529 (A-E) Stable isotope tracing of WT and MLL3/4 DKO ESCs labeled with [$^{13}C_6$]-glucose. The
530 levels of isotopologues (m+0 to m+6) of citrate/isocitrate (A), α-KG (B), succinate (C), fumarate
531 (D), and malate (E) were shown as stacked bar plots.
532 (F-K) Stable isotope tracing of WT and MLL3/4 DKO ESCs labeled with [$^{13}C_5$]-glutamine. The
533 levels of isotopologues (m+0 to m+6) of glutamate (F), α-KG (G), succinate (H), fumarate (I),
534 malate (J), and citrate/isocitrate (K) were shown as stacked bar plots.
535 (L) Relative expression levels of genes coding TCA-cycle enzymes involved in the anabolism and
536 catabolism of α-KG, succinate, fumarate, and malate. CPM (counts per million reads) from RNA-

537 seq data (*14*) of MLL3/4 DKO ESCs were normalized to those of WT ESCs. p-values were
538 determined by two-sided Wald test and corrected using the Benjamini–Hochberg method.
539 (M-O) Western blots showing levels of OGDH (M), Succinyl-CoA Synthetase subunits (N), SDHA
540 (O, top blot), and FH (O, middle blot). 10 and 20μg of cell lysates were loaded for each sample.
541 Experiments were repeated three times independently and representative results were shown.
542 Protein levels in each lane were quantified by normalizing with Tubulin or HSP90 signals of the
543 corresponding lane.
544
545 **Figure S3. HK2 overexpression leads to an increase in the glycolytic activity but a decrease**
546 **in mitochondrial respiration in MLL3/4 DKO ESCs.**
547 (A) Western blots showing the induction of 3×HA-tagged HK2 in HK2-overexpressing MLL3/4
548 DKO ESCs by DOX. 10 and 20μg of cell lysates were loaded for each sample. Experiments were
549 repeated three times independently and representative results were shown. Protein levels of HK2
550 in each lane were quantified by normalizing with Tubulin signals of the corresponding lane.
551 (B) Representative ECAR traces of MLL3/4 DKO ESCs treated with DOX (DKO+DOX) and
552 MLL3/4 DKO ESCs overexpressing HK2 (3×HA-HK2+DOX) measured by the Seahorse XF
553 glycolysis stress test assay. Data were normalized by the number of cells at the time of the assay
554 and are represented as mean ± S.D. Each data point had six replicates, and the experiment was
555 repeated three times independently.
556 (C-D) Bar plots of ECAR showing the levels of glycolysis (C) and glycolytic capacity (D) in
557 MLL3/4 DKO ESCs treated with DOX (DKO+DOX) and MLL3/4 DKO ESCs overexpressing
558 HK2 (3×HA-HK2+DOX). Data are presented as mean ± S.D. p-values were calculated using
559 Student's t-test.

560 (E) Representative OCR traces of MLL3/4 DKO ESCs treated with DOX (DKO+DOX) and
561 MLL3/4 DKO ESCs overexpressing HK2 (3×HA-HK2+DOX) measured by the Seahorse XF
562 mitochondrial stress test assay. Data were normalized by the number of cells at the time of the
563 assay and are represented as mean ± S.D. Each data point had six replicates, and the experiment
564 was repeated three times independently.
565 (F-G) Bar plots showing the OCR levels in MLL3/4 DKO ESCs treated with DOX (DKO+DOX)
566 and MLL3/4 DKO ESCs overexpressing HK2 (3×HA-HK2+DOX) during basal (F) and maximal
567 (G) respiration. Data are presented as mean ± S.D. p-values were calculated using Student's t-test.
568
569 **Figure S4. Stable isotope tracing of MLL3/4 DKO ESCs treated with DOX (DKO+DOX) and**
570 **MLL3/4 DKO ESCs overexpressing HK2/OGDH (DOE+DOX) labeled with [$^{13}C_6$]-glucose.**
571 The levels of isotopologues of F6P/G1P/G6P (A, m+0 to m+6), lactate (B m+0 to m+3),
572 citrate/isocitrate (m+2 in C and m+0 to m+6 in D), α-KG (E, m+0 to m+5), succinate (F, m+0 to
573 m+4), fumarate (G, m+0 to m+4), and malate (H, m+0 to m+4) were shown.
574
575 **Figure S5. The impact of MLL3/4 loss and HK2/OGDH overexpression on the expression**
576 **levels of marker genes of pluripotency and differentiation in EBs.**
577 (A-B) Relative expression levels of pluripotency genes (A) and differentiation markers (B) in
578 MLL3/4 DKO EBs compared with WT EBs. Log2 fold change of RNA-seq signals (CPM) were
579 shown. Data are presented as mean values ± SD. n = 2 biologically independent experiments. All
580 p-values were smaller than 0.01 compared with WT EBs.
581 (C-D) Relative expression levels of pluripotency genes (C) and differentiation markers (D) in
582 MLL3/4 DKO EBs overexpressing HK2/OGDH (DOE+DOX) compared with MLL3/4 DKO EBs

583 treated with DOX (DKO+DOX). Log2 fold change of RNA-seq signals (CPM) were shown. Data
584 are presented as mean values ± SD. n = 2 biologically independent experiments. All p-values were
585 smaller than 0.01 compared with DKO+DOX EBs.
586

587 **References**

588

589 1. S. B. Ng, A. W. Bigham, K. J. Buckingham, M. C. Hannibal, M. J. McMillin, H. I.
590 Gildersleeve, A. E. Beck, H. K. Tabor, G. M. Cooper, H. C. Mefford, C. Lee, E. H. Turner,
591 J. D. Smith, M. J. Rieder, K. Yoshiura, N. Matsumoto, T. Ohta, N. Niikawa, D. A.
592 Nickerson, M. J. Bamshad, J. Shendure, Exome sequencing identifies MLL2 mutations
593 as a cause of Kabuki syndrome. *Nat Genet* **42**, 790-793 (2010).
594 2. I. D. Krantz, J. McCallum, C. DeScipio, M. Kaur, L. A. Gillis, D. Yaeger, L. Jukofsky, N.
595 Wasserman, A. Bottani, C. A. Morris, M. J. Nowaczyk, H. Toriello, M. J. Bamshad, J. C.
596 Carey, E. Rappaport, S. Kawauchi, A. D. Lander, A. L. Calof, H. H. Li, M. Devoto, L. G.
597 Jackson, Cornelia de Lange syndrome is caused by mutations in NIPBL, the human
598 homolog of Drosophila melanogaster Nipped-B. *Nat Genet* **36**, 631-635 (2004).
599 3. E. K. Schorry, M. Keddache, N. Lanphear, J. H. Rubinstein, S. Srodulski, D. Fletcher, R.
600 I. Blough-Pfau, G. A. Grabowski, Genotype-phenotype correlations in Rubinstein-
601 Taybi syndrome. *Am J Med Genet A* **146A**, 2512-2519 (2008).
602 4. T. S. Koemans, T. Kleefstra, M. C. Chubak, M. H. Stone, M. R. F. Reijnders, S. de Munnik,
603 M. H. Willemsen, M. Fenckova, C. Stumpel, L. A. Bok, M. Sifuentes Saenz, K. A. Byerly,
604 L. B. Baughn, A. P. A. Stegmann, R. Pfundt, H. Zhou, H. van Bokhoven, A. Schenck, J.
605 M. Kramer, Functional convergence of histone methyltransferases EHMT1 and
606 KMT2C involved in intellectual disability and autism spectrum disorder. *PLoS Genet*
607 **13**, e1006864 (2017).
608 5. D. Hu, X. Gao, M. A. Morgan, H. M. Herz, E. R. Smith, A. Shilatifard, The MLL3/MLL4
609 branches of the COMPASS family function as major histone H3K4 monomethylases
610 at enhancers. *Mol Cell Biol* **33**, 4745-4754 (2013).
611 6. R. Rickels, H. M. Herz, C. C. Sze, K. Cao, M. A. Morgan, C. K. Collings, M. Gause, Y. H.
612 Takahashi, L. Wang, E. J. Rendleman, S. A. Marshall, A. Krueger, E. T. Bartom, A. Piunti,
613 E. R. Smith, N. A. Abshiru, N. L. Kelleher, D. Dorsett, A. Shilatifard, Histone H3K4
614 monomethylation catalyzed by Trr and mammalian COMPASS-like proteins at
615 enhancers is dispensable for development and viability. *Nat Genet* **49**, 1647-1653
616 (2017).
617 7. K. Cao, C. K. Collings, M. A. Morgan, S. A. Marshall, E. J. Rendleman, P. A. Ozark, E. R.
618 Smith, A. Shilatifard, An Mll4/COMPASS-Lsd1 epigenetic axis governs enhancer
619 function and pluripotency transition in embryonic stem cells. *Sci Adv* **4**, eaap8747
620 (2018).
621 8. A. Shilatifard, The COMPASS family of histone H3K4 methylases: mechanisms of
622 regulation in development and disease pathogenesis. *Annu Rev Biochem* **81**, 65-95
623 (2012).
624 9. N. D. Heintzman, R. K. Stuart, G. Hon, Y. Fu, C. W. Ching, R. D. Hawkins, L. O. Barrera,
625 S. Van Calcar, C. Qu, K. A. Ching, W. Wang, Z. Weng, R. D. Green, G. E. Crawford, B.
626 Ren, Distinct and predictive chromatin signatures of transcriptional promoters and
627 enhancers in the human genome. *Nat Genet* **39**, 311-318 (2007).

10. J. E. Lee, C. Wang, S. Xu, Y. W. Cho, L. Wang, X. Feng, A. Baldridge, V. Sartorelli, L. Zhuang, W. Peng, K. Ge, H3K4 mono- and di-methyltransferase MLL4 is required for enhancer activation during cell differentiation. *Elife* **2**, e01503 (2013).
11. D. Ashokkumar, Q. Zhang, C. Much, A. S. Bledau, R. Naumann, D. Alexopoulou, A. Dahl, N. Goveas, J. Fu, K. Anastassiadis, A. F. Stewart, A. Kranz, MLL4 is required after implantation, whereas MLL3 becomes essential during late gestation. *Development* **147**, (2020).
12. V. Faundes, W. G. Newman, L. Bernardini, N. Canham, J. Clayton-Smith, B. Dallapiccola, S. J. Davies, M. K. Demos, A. Goldman, H. Gill, R. Horton, B. Kerr, D. Kumar, A. Lehman, S. McKee, J. Morton, M. J. Parker, J. Rankin, L. Robertson, I. K. Temple, S. Clinical Assessment of the Utility of, S. Evaluation as a Service, S. Deciphering Developmental Disorders, S. Banka, Histone Lysine Methylases and Demethylases in the Landscape of Human Developmental Disorders. *Am J Hum Genet* **102**, 175-187 (2018).
13. D. Rots, S. Choufani, V. Faundes, A. J. M. Dingemans, S. Joss, N. Foulds, E. A. Jones, S. Stewart, P. Vasudevan, T. Dabir, S. M. Park, R. Jewell, N. Brown, L. Pais, S. Jacquemont, K. Jizi, C. Ravenswaaij-Arts, H. Y. Kroes, C. Stumpel, C. W. Ockeloen, I. J. Diets, M. Nizon, M. Vincent, B. Cogne, T. Besnard, M. Kambouris, E. Anderson, E. H. Zackai, C. McDougall, S. Donoghue, A. O'Donnell-Luria, Z. Valivullah, M. O'Leary, S. Srivastava, H. Byers, N. Leslie, S. Mazzola, G. E. Tiller, M. Vera, J. J. Shen, R. Boles, V. Jain, E. Brischoux-Boucher, E. Kinning, B. N. Simpson, J. C. Giltay, J. Harris, B. Keren, A. Guimier, P. Marijon, B. B. A. Vries, C. S. Motter, B. A. Mendelsohn, S. Coffino, E. H. Gerkes, A. Afenjar, P. Visconti, E. Bacchelli, E. Maestrini, A. Delahaye-Duriez, C. Gooch, Y. Hendriks, H. Adams, C. Thauvin-Robinet, S. Josephi-Taylor, M. Bertoli, M. J. Parker, J. W. Rutten, O. Caluseriu, H. J. Vernon, J. Kaziyev, J. Zhu, J. Kremen, Z. Frazier, H. Osika, D. Breault, S. Nair, S. M. E. Lewis, F. Ceroni, M. Viggiano, A. Posar, H. Brittain, T. Giovanna, G. Giulia, L. Quteineh, R. Ha-Vinh Leuchter, E. Zonneveld-Huijssoon, C. Mellado, I. Marey, A. Coudert, M. I. Aracena Alvarez, M. G. P. Kennis, A. Bouman, M. Roifman, M. I. Amoros Rodriguez, J. D. Ortigoza-Escobar, V. Vernimmen, M. Sinnema, R. Pfundt, H. G. Brunner, L. Vissers, T. Kleefstra, R. Weksberg, S. Banka, Pathogenic variants in KMT2C result in a neurodevelopmental disorder distinct from Kleefstra and Kabuki syndromes. *Am J Hum Genet* **111**, 1626-1642 (2024).
14. Z. Zhao, K. Cao, J. Watanabe, C. N. Philips, J. M. Zeidner, Y. Ishi, Q. Wang, S. R. Gold, K. Junkins, E. T. Bartom, F. Yue, N. S. Chandel, R. Hashizume, I. Ben-Sahra, A. Shilatifard, Therapeutic targeting of metabolic vulnerabilities in cancers with MLL3/4-COMPASS epigenetic regulator mutations. *J Clin Invest* **133**, (2023).
15. H. Alam, M. Tang, M. Maitituoheti, S. S. Dhar, M. Kumar, C. Y. Han, C. R. Ambati, S. B. Amin, B. Gu, T. Y. Chen, Y. H. Lin, J. Chen, F. L. Muller, N. Putluri, E. R. Flores, F. J. DeMayo, L. Baseler, K. Rai, M. G. Lee, KMT2D Deficiency Impairs Super-Enhancers to Confer a Glycolytic Vulnerability in Lung Cancer. *Cancer Cell* **37**, 599-617 e597 (2020).
16. M. Maitituoheti, E. Z. Keung, M. Tang, L. Yan, H. Alam, G. Han, A. K. Singh, A. T. Raman, C. Terranova, S. Sarkar, E. Orouji, S. B. Amin, S. Sharma, M. Williams, N. S. Samant, M. Dhamdhere, N. Zheng, T. Shah, A. Shah, J. B. Axelrad, N. E. Anvar, Y. H. Lin, S. Jiang, E. Q. Chang, D. R. Ingram, W. L. Wang, A. Lazar, M. G. Lee, F. Muller, L. Wang, H. Ying,

K. Rai, Enhancer Reprogramming Confers Dependence on Glycolysis and IGF Signaling in KMT2D Mutant Melanoma. *Cell Rep* **33**, 108293 (2020).

17. W. Zhou, M. Choi, D. Margineantu, L. Margaretha, J. Hesson, C. Cavanaugh, C. A. Blau, M. S. Horwitz, D. Hockenbery, C. Ware, H. Ruohola-Baker, HIF1alpha induced switch from bivalent to exclusively glycolytic metabolism during ESC-to-EpiSC/hESC transition. *EMBO J* **31**, 2103-2116 (2012).
18. C. D. Folmes, T. J. Nelson, A. Martinez-Fernandez, D. K. Arrell, J. Z. Lindor, P. P. Dzeja, Y. Ikeda, C. Perez-Terzic, A. Terzic, Somatic oxidative bioenergetics transitions into pluripotency-dependent glycolysis to facilitate nuclear reprogramming. *Cell Metab* **14**, 264-271 (2011).
19. A. D. Panopoulos, O. Yanes, S. Ruiz, Y. S. Kida, D. Diep, R. Tautenhahn, A. Herrerias, E. M. Batchelder, N. Plongthongkum, M. Lutz, W. T. Berggren, K. Zhang, R. M. Evans, G. Siuzdak, J. C. Izpisua Belmonte, The metabolome of induced pluripotent stem cells reveals metabolic changes occurring in somatic cell reprogramming. *Cell Res* **22**, 168-177 (2012).
20. A. Moussaieff, M. Rouleau, D. Kitsberg, M. Cohen, G. Levy, D. Barasch, A. Nemirovski, S. Shen-Orr, I. Laevsky, M. Amit, D. Bomze, B. Elena-Herrmann, T. Scherf, M. Nissim-Rafinia, S. Kempa, J. Itskovitz-Eldor, E. Meshorer, D. Aberdam, Y. Nahmias, Glycolysis-mediated changes in acetyl-CoA and histone acetylation control the early differentiation of embryonic stem cells. *Cell Metab* **21**, 392-402 (2015).
21. A. De Los Angeles, F. Ferrari, R. Xi, Y. Fujiwara, N. Benvenisty, H. Deng, K. Hochedlinger, R. Jaenisch, S. Lee, H. G. Leitch, M. W. Lensch, E. Lujan, D. Pei, J. Rossant, M. Wernig, P. J. Park, G. Q. Daley, Hallmarks of pluripotency. *Nature* **525**, 469-478 (2015).
22. P. Du, J. Wu, Hallmarks of totipotent and pluripotent stem cell states. *Cell Stem Cell* **31**, 312-333 (2024).
23. C. Buecker, R. Srinivasan, Z. Wu, E. Calo, D. Acampora, T. Faial, A. Simeone, M. Tan, T. Swigut, J. Wysocka, Reorganization of enhancer patterns in transition from naive to primed pluripotency. *Cell Stem Cell* **14**, 838-853 (2014).
24. C. Zeng, J. Chen, E. W. Cooke, A. Subuddhi, E. T. Roodman, F. X. Chen, K. Cao, Demethylase-independent roles of LSD1 in regulating enhancers and cell fate transition. *Nat Commun* **14**, 4944 (2023).
25. E. A. Rowland, T. M. Greco, C. K. Snowden, A. L. McCabe, T. J. Silhavy, I. M. Cristea, Sirtuin Lipoamidase Activity Is Conserved in Bacteria as a Regulator of Metabolic Enzyme Complexes. *mBio* **8**, (2017).
26. E. A. Rowland, C. K. Snowden, I. M. Cristea, Protein lipoylation: an evolutionarily conserved metabolic regulator of health and disease. *Curr Opin Chem Biol* **42**, 76-85 (2018).
27. J. E. Cronan, Assembly of Lipoic Acid on Its Cognate Enzymes: an Extraordinary and Essential Biosynthetic Pathway. *Microbiol Mol Biol Rev* **80**, 429-450 (2016).
28. P. S. J. Bailey, B. M. Ortmann, A. W. Martinelli, J. W. Houghton, A. S. H. Costa, S. P. Burr, R. Antrobus, C. Frezza, J. A. Nathan, ABHD11 maintains 2-oxoglutarate metabolism by preserving functional lipoylation of the 2-oxoglutarate dehydrogenase complex. *Nat Commun* **11**, 4046 (2020).

29. J. A. Lessard, G. R. Crabtree, Chromatin regulatory mechanisms in pluripotency. *Annu Rev Cell Dev Biol* **26**, 503-532 (2010).
30. S. Feng, S. E. Jacobsen, W. Reik, Epigenetic reprogramming in plant and animal development. *Science* **330**, 622-627 (2010).
31. B. Papp, K. Plath, Epigenetics of reprogramming to induced pluripotency. *Cell* **152**, 1324-1343 (2013).
32. W. W. Tee, D. Reinberg, Chromatin features and the epigenetic regulation of pluripotency states in ESCs. *Development* **141**, 2376-2390 (2014).
33. S. Schlesinger, E. Meshorer, Open Chromatin, Epigenetic Plasticity, and Nuclear Organization in Pluripotency. *Dev Cell* **48**, 135-150 (2019).
34. A. Burton, M. E. Torres-Padilla, Epigenome dynamics in early mammalian embryogenesis. *Nat Rev Genet* **26**, 587-603 (2025).
35. X. Wan, S. Zhang, J. Li, D. Kong, M. Chen, Epigenetic remodeling during early embryonic development. *Front Cell Dev Biol* **14**, 1750381 (2026).
36. R. Eskeland, M. Leeb, G. R. Grimes, C. Kress, S. Boyle, D. Sproul, N. Gilbert, Y. Fan, A. I. Skoultchi, A. Wutz, W. A. Bickmore, Ring1B compacts chromatin structure and represses gene expression independent of histone ubiquitination. *Mol Cell* **38**, 452-464 (2010).
37. R. S. Illingworth, M. Moffat, A. R. Mann, D. Read, C. J. Hunter, M. M. Pradeepa, I. R. Adams, W. A. Bickmore, The E3 ubiquitin ligase activity of RING1B is not essential for early mouse development. *Genes Dev* **29**, 1897-1902 (2015).
38. C. C. Sze, K. Cao, C. K. Collings, S. A. Marshall, E. J. Rendleman, P. A. Ozark, F. X. Chen, M. A. Morgan, L. Wang, A. Shilatifard, Histone H3K4 methylation-dependent and -independent functions of Set1A/COMPASS in embryonic stem cell self-renewal and differentiation. *Genes Dev* **31**, 1732-1737 (2017).
39. L. Wang, C. K. Collings, Z. Zhao, K. A. Cozzolino, Q. Ma, K. Liang, S. A. Marshall, C. C. Sze, R. Hashizume, J. N. Savas, A. Shilatifard, A cytoplasmic COMPASS is necessary for cell survival and triple-negative breast cancer pathogenesis by regulating metabolism. *Genes Dev* **31**, 2056-2066 (2017).
40. K. M. Dorighi, T. Swigut, T. Henriques, N. V. Bhanu, B. S. Scruggs, N. Nady, C. D. Still, 2nd, B. A. Garcia, K. Adelman, J. Wysocka, Mll3 and Mll4 Facilitate Enhancer RNA Synthesis and Transcription from Promoters Independently of H3K4 Monomethylation. *Mol Cell* **66**, 568-576 e564 (2017).
41. K. Cao, M. Ugarenko, P. A. Ozark, J. Wang, S. A. Marshall, E. J. Rendleman, K. Liang, L. Wang, L. Zou, E. R. Smith, F. Yue, A. Shilatifard, DOT1L-controlled cell-fate determination and transcription elongation are independent of H3K79 methylation. *Proc Natl Acad Sci U S A* **117**, 27365-27373 (2020).
42. M. A. J. Morgan, A. Shilatifard, Epigenetic moonlighting: Catalytic-independent functions of histone modifiers in regulating transcription. *Sci Adv* **9**, eadg6593 (2023).
43. A. Khan, C. Zhang, P. G. Nguyen, J. M. Metts, L. C. Collins, K. Jain, C. A. Mills, L. Vlach, K. Li, A. L. Brademeyer, B. M. Bowman, M. B. Major, J. Aube, L. E. Herring, W. K. Rathmell, F. M. Mason, I. J. Davis, Q. Zhang, B. D. Strahl, A SETD2-CDK1-lamin axis maintains nuclear morphology and genome stability. *Nat Cell Biol* **27**, 1327-1341 (2025).

44. C. Wang, J. E. Lee, B. Lai, T. S. Macfarlan, S. Xu, L. Zhuang, C. Liu, W. Peng, K. Ge, Enhancer priming by H3K4 methyltransferase MLL4 controls cell fate transition. *Proc Natl Acad Sci U S A* **113**, 11871-11876 (2016).
45. C. C. Sze, A. Shilatifard, MLL3/MLL4/COMPASS Family on Epigenetic Regulation of Enhancer Function and Cancer. *Cold Spring Harb Perspect Med* **6**, (2016).
46. G. Xie, J. E. Lee, A. D. Senft, Y. K. Park, Y. Jang, S. Chakraborty, J. J. Thompson, K. McKernan, C. Liu, T. S. Macfarlan, P. P. Rocha, W. Peng, K. Ge, MLL3/MLL4 methyltransferase activities control early embryonic development and embryonic stem cell differentiation in a lineage-selective manner. *Nat Genet* **55**, 693-705 (2023).
47. J. W. Hong, D. A. Hendrix, M. S. Levine, Shadow enhancers as a source of evolutionary novelty. *Science* **321**, 1314 (2008).
48. K. Cao, C. K. Collings, S. A. Marshall, M. A. Morgan, E. J. Rendleman, L. Wang, C. C. Sze, T. Sun, E. T. Bartom, A. Shilatifard, SET1A/COMPASS and shadow enhancers in the regulation of homeotic gene expression. *Genes Dev* **31**, 787-801 (2017).
49. E. Z. Kvon, R. Waymack, M. Gad, Z. Wunderlich, Enhancer redundancy in development and disease. *Nat Rev Genet* **22**, 324-336 (2021).
50. Y. Tsukada, J. Fang, H. Erdjument-Bromage, M. E. Warren, C. H. Borchers, P. Tempst, Y. Zhang, Histone demethylation by a family of JmjC domain-containing proteins. *Nature* **439**, 811-816 (2006).
51. M. Tahiliani, K. P. Koh, Y. Shen, W. A. Pastor, H. Bandukwala, Y. Brudno, S. Agarwal, L. M. Iyer, D. R. Liu, L. Aravind, A. Rao, Conversion of 5-methylcytosine to 5-hydroxymethylcytosine in mammalian DNA by MLL partner TET1. *Science* **324**, 930-935 (2009).
52. W. Xu, H. Yang, Y. Liu, Y. Yang, P. Wang, S. H. Kim, S. Ito, C. Yang, P. Wang, M. T. Xiao, L. X. Liu, W. Q. Jiang, J. Liu, J. Y. Zhang, B. Wang, S. Frye, Y. Zhang, Y. H. Xu, Q. Y. Lei, K. L. Guan, S. M. Zhao, Y. Xiong, Oncometabolite 2-hydroxyglutarate is a competitive inhibitor of alpha-ketoglutarate-dependent dioxygenases. *Cancer Cell* **19**, 17-30 (2011).
53. M. Xiao, H. Yang, W. Xu, S. Ma, H. Lin, H. Zhu, L. Liu, Y. Liu, C. Yang, Y. Xu, S. Zhao, D. Ye, Y. Xiong, K. L. Guan, Inhibition of alpha-KG-dependent histone and DNA demethylases by fumarate and succinate that are accumulated in mutations of FH and SDH tumor suppressors. *Genes Dev* **26**, 1326-1338 (2012).
54. K. Skvortsova, E. Masle-Farquhar, P. L. Luu, J. Z. Song, W. Qu, E. Zotenko, C. M. Gould, Q. Du, T. J. Peters, Y. Colino-Sanguino, R. Pidsley, S. S. Nair, A. Khoury, G. C. Smith, L. A. Miosge, J. H. Reed, J. G. Kench, M. A. Rubin, L. Horvath, O. Bogdanovic, S. M. Lim, J. M. Polo, C. C. Goodnow, C. Stirzaker, S. J. Clark, DNA Hypermethylation Encroachment at CpG Island Borders in Cancer Is Predisposed by H3K4 Monomethylation Patterns. *Cancer Cell* **35**, 297-314 e298 (2019).
55. E. W. Cooke, C. Zeng, S. M. Nur, Y. Jia, A. Huang, J. Chen, P. Gao, F. X. Chen, F. Jin, K. Cao, H3K79 methylation and H3K36 trimethylation synergistically regulate gene expression in pluripotent stem cells. *Sci Adv* **11**, eadt8765 (2025).
56. A. M. Bolger, M. Lohse, B. Usadel, Trimmomatic: a flexible trimmer for Illumina sequence data. *Bioinformatics* **30**, 2114-2120 (2014).

57. A. Dobin, C. A. Davis, F. Schlesinger, J. Drenkow, C. Zaleski, S. Jha, P. Batut, M. Chaisson, T. R. Gingeras, STAR: ultrafast universal RNA-seq aligner. *Bioinformatics* **29**, 15-21 (2013).
58. F. Ramirez, D. P. Ryan, B. Gruning, V. Bhardwaj, F. Kilpert, A. S. Richter, S. Heyne, F. Dundar, T. Manke, deepTools2: a next generation web server for deep-sequencing data analysis. *Nucleic Acids Res* **44**, W160-165 (2016).
59. S. Anders, P. T. Pyl, W. Huber, HTSeq--a Python framework to work with high-throughput sequencing data. *Bioinformatics* **31**, 166-169 (2015).
60. M. D. Robinson, D. J. McCarthy, G. K. Smyth, edgeR: a Bioconductor package for differential expression analysis of digital gene expression data. *Bioinformatics* **26**, 139-140 (2010).
61. T. Wu, E. Hu, S. Xu, M. Chen, P. Guo, Z. Dai, T. Feng, L. Zhou, W. Tang, L. Zhan, X. Fu, S. Liu, X. Bo, G. Yu, clusterProfiler 4.0: A universal enrichment tool for interpreting omics data. *Innovation (Camb)* **2**, 100141 (2021).
62. Y. Zhou, B. Zhou, L. Pache, M. Chang, A. H. Khodabakhshi, O. Tanaseichuk, C. Benner, S. K. Chanda, Metascape provides a biologist-oriented resource for the analysis of systems-level datasets. *Nat Commun* **10**, 1523 (2019).

Figure 1

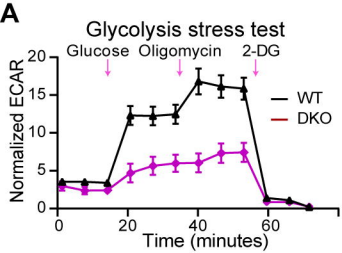
A
Glycolysis stress test
Glucose
Oligomycin
2-DG
Normalized ECAR
Time (minutes)
WT
DKO

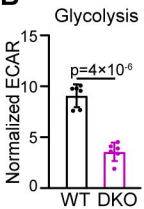
B
Glycolysis
Normalized ECAR
p=4×10-6
WT
DKO

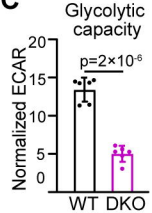
C
Glycolytic capacity
Normalized ECAR
p=2×10-6
WT
DKO

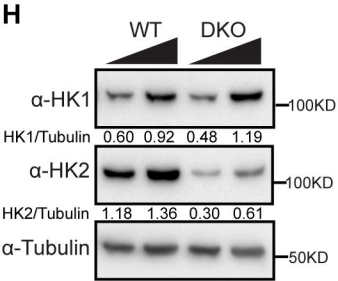
H
WT
DKO
α-HK1
100KD
HK1/Tubulin
0.60
0.92
0.48
1.19
α-HK2
100KD
HK2/Tubulin
1.18
1.36
0.30
0.61
α-Tubulin
50KD

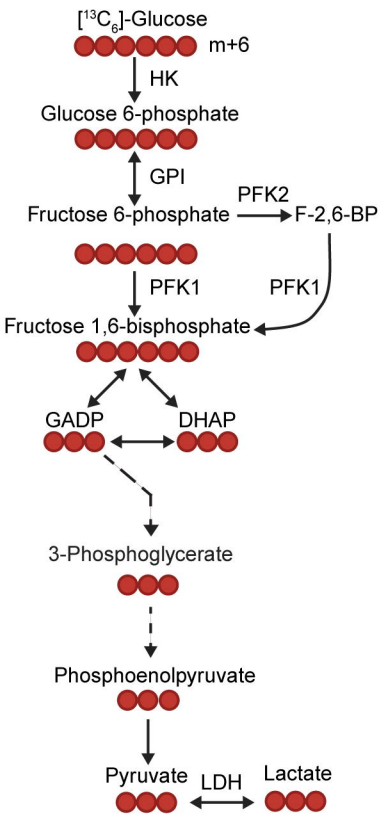
D
[13C6]-Glucose
m+6
HK
Glucose 6-phosphate
GPI
Fructose 6-phosphate
PFK2
F-2,6-BP
PFK1
PFK1
Fructose 1,6-bisphosphate
GADP
DHAP
3-Phosphoglycerate
Phosphoenolpyruvate
Pyruvate
LDH
Lactate

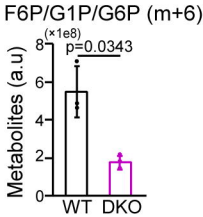
E
F6P/G1P/G6P (m+6)
(×1e8)
p=0.0343
Metabolites (a.u)
WT
DKO

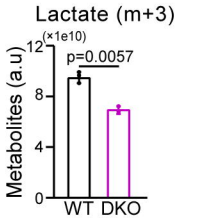
F
Lactate (m+3)
(×1e10)
p=0.0057
Metabolites (a.u)
WT
DKO

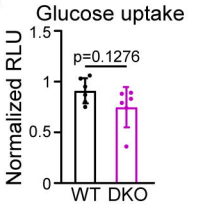
G
Glucose uptake
p=0.1276
Normalized RLU
WT
DKO

Figure 2

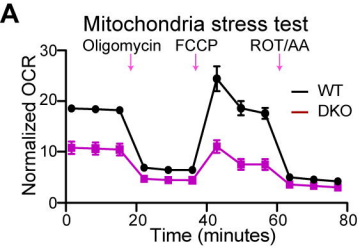
A
Mitochondria stress test
Oligomycin
FCCP
ROT/AA
Normalized OCR
Time (minutes)
WT
DKO

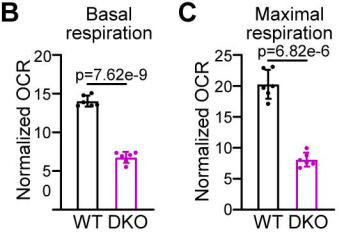
B
Basal respiration
p=7.62e-9
Normalized OCR
WT DKO
C
Maximal respiration
p=6.82e-6
Normalized OCR
WT DKO

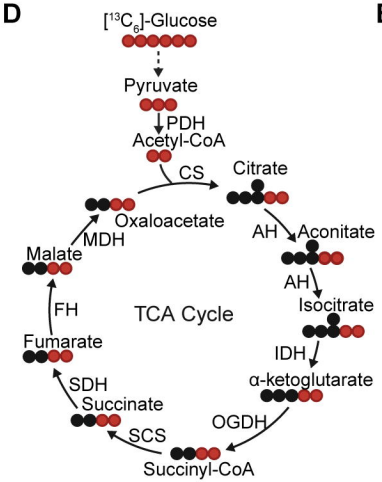
D
[13C6]-Glucose
Pyruvate
PDH
Acetyl-CoA
CS
Citrate
AH
Aconitate
AH
Isocitrate
IDH
α-ketoglutarate
OGDH
Succinyl-CoA
SCS
Succinate
SDH
Fumarate
FH
Malate
MDH
Oxaloacetate
TCA Cycle

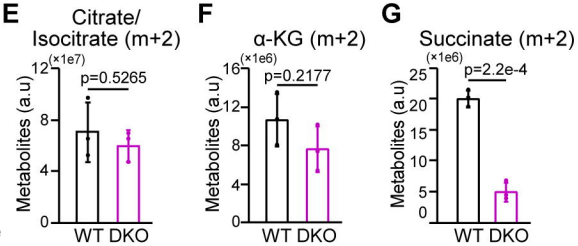
E
Citrate/ Isocitrate (m+2)
p=0.5265
F
α-KG (m+2)
p=0.2177
G
Succinate (m+2)
p=2.2e-4
Metabolites (a.u)
WT DKO

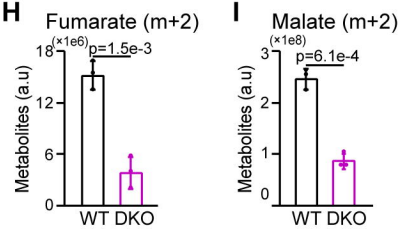
H
Fumarate (m+2)
p=1.5e-3
I
Malate (m+2)
p=6.1e-4
Metabolites (a.u)
WT DKO

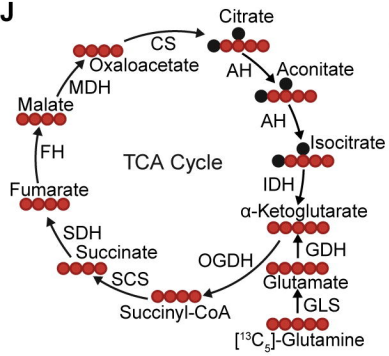
J
Citrate
CS
Oxaloacetate
MDH
Malate
AH
Aconitate
AH
Isocitrate
FH
TCA Cycle
IDH
Fumarate
α-Ketoglutarate
SDH
Succinate
OGDH
GDH
SCS
Glutamate
Succinyl-CoA
GLS
[13C5]-Glutamine

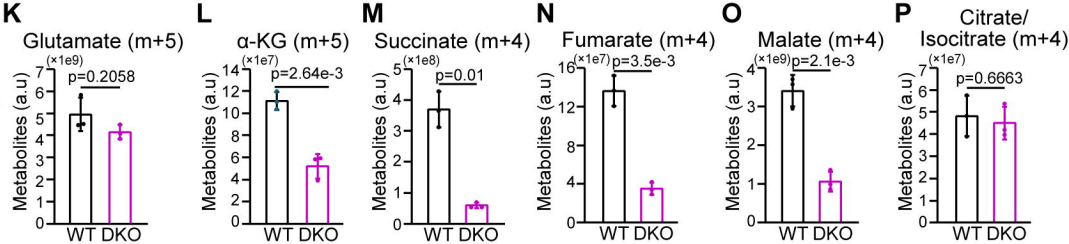
K
Glutamate (m+5)
p=0.2058
L
α-KG (m+5)
p=2.64e-3
M
Succinate (m+4)
p=0.01
N
Fumarate (m+4)
p=3.5e-3
O
Malate (m+4)
p=2.1e-3
P
Citrate/ Isocitrate (m+4)
p=0.6663
Metabolites (a.u)
WT DKO

Figure 3

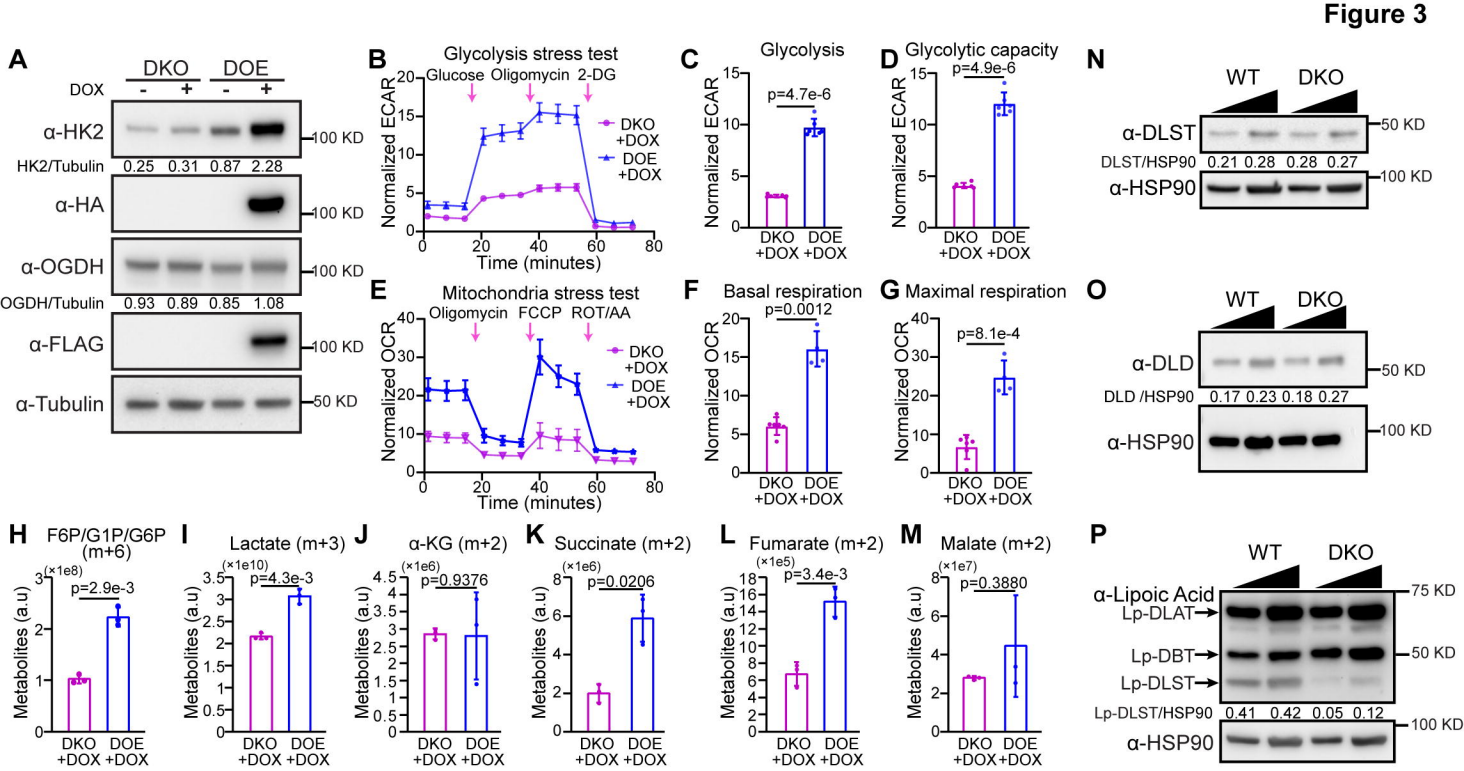
A
DKO
DOE
DOX
- + - +
α-HK2
100 KD
HK2/Tubulin
0.25 0.31 0.87 2.28
α-HA
100 KD
α-OGDH
100 KD
OGDH/Tubulin
0.93 0.89 0.85 1.08
α-FLAG
100 KD
α-Tubulin
50 KD
B
Glycolysis stress test
Glucose Oligomycin 2-DG
Normalized ECAR
Time (minutes)
DKO +DOX
DOE +DOX
C
Glycolysis
p=4.7e-6
Normalized ECAR
DKO +DOX
DOE +DOX
D
Glycolytic capacity
p=4.9e-6
Normalized ECAR
E
Mitochondria stress test
Oligomycin FCCP ROT/AA
Normalized OCR
Time (minutes)
F
Basal respiration
p=0.0012
Normalized OCR
G
Maximal respiration
p=8.1e-4
Normalized OCR
N
WT DKO
α-DLST
50 KD
DLST/HSP90
0.21 0.28 0.28 0.27
α-HSP90
100 KD
O
WT DKO
α-DLD
50 KD
DLD /HSP90
0.17 0.23 0.18 0.27
α-HSP90
100 KD
H
F6P/G1P/G6P (m+6)
(×1e8)
p=2.9e-3
Metabolites (a.u)
I
Lactate (m+3)
(×1e10)
p=4.3e-3
J
α-KG (m+2)
(×1e6)
p=0.9376
K
Succinate (m+2)
(×1e6)
p=0.0206
L
Fumarate (m+2)
(×1e5)
p=3.4e-3
M
Malate (m+2)
(×1e7)
p=0.3880
P
WT DKO
α-Lipoic Acid
Lp-DLAT
Lp-DBT
Lp-DLST
75 KD
50 KD
Lp-DLST/HSP90
0.41 0.42 0.05 0.12
α-HSP90
100 KD

Figure 4

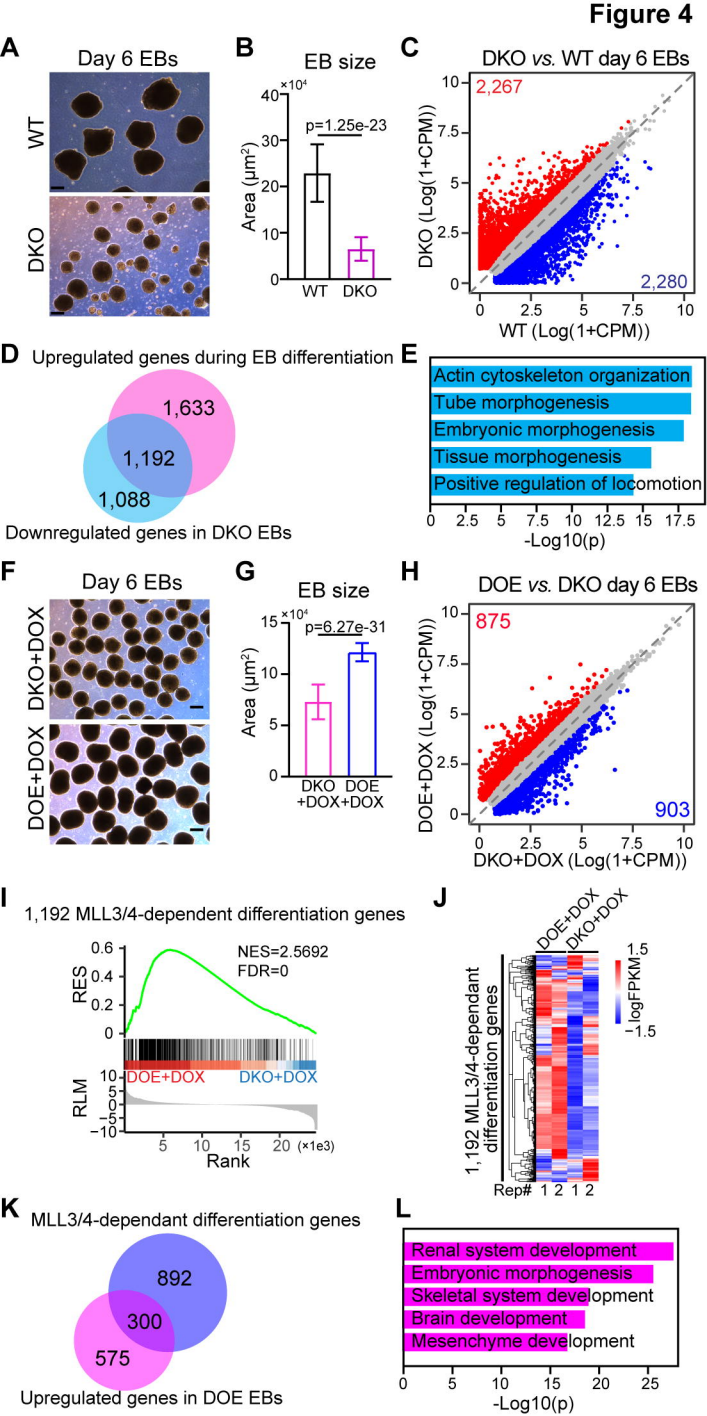
A
Day 6 EBs
WT
DKO
B
EB size
×10⁴
Area (μm²)
p=1.25e-23
WT
DKO
C
DKO vs. WT day 6 EBs
2,267
2,280
DKO (Log(1+CPM))
WT (Log(1+CPM))
D
Upregulated genes during EB differentiation
1,633
1,192
1,088
Downregulated genes in DKO EBs
E
Actin cytoskeleton organization
Tube morphogenesis
Embryonic morphogenesis
Tissue morphogenesis
Positive regulation of locomotion
-Log10(p)
F
Day 6 EBs
DKO+DOX
DOE+DOX
G
EB size
×10⁴
Area (μm²)
p=6.27e-31
DKO +DOX
DOE +DOX
H
DOE vs. DKO day 6 EBs
875
903
DOE+DOX (Log(1+CPM))
DKO+DOX (Log(1+CPM))
I
1,192 MLL3/4-dependent differentiation genes
NES=2.5692
FDR=0
RES
RLM
DOE+DOX
DKO+DOX
Rank
(×1e3)
J
DOE+DOX
DKO+DOX
1,192 MLL3/4-dependant differentiation genes
-logFPKM
Rep# 1 2 1 2
K
MLL3/4-dependant differentiation genes
892
300
575
Upregulated genes in DOE EBs
L
Renal system development
Embryonic morphogenesis
Skeletal system development
Brain development
Mesenchyme development
-Log10(p)